PNAS RESEARCH ARTICLE | APPLIED MATHEMATICS

Bifurcation instructed design of multistate machines

Teaya Yang[a,1], David Hathcock[a,1], Yuchao Chen[a], Paul L. McEuen[a,b], James P. Sethna[a], Itai Cohen[a,b], and Itay Griniasty[a,2]

Edited by Herbert Levine, Northeastern University, Boston, MA; received January 3, 2023; accepted July 23, 2023

We propose a design paradigm for multistate machines where transitions from one state to another are organized by bifurcations of multiple equilibria of the energy landscape describing the collective interactions of the machine components. This design paradigm is attractive since, near bifurcations, small variations in a few control parameters can result in large changes to the system's state providing an emergent lever mechanism. Further, the topological configuration of transitions between states near such bifurcations ensures robust operation, making the machine less sensitive to fabrication errors and noise. To design such machines, we develop and implement a new efficient algorithm that searches for interactions between the machine components that give rise to energy landscapes with these bifurcation structures. We demonstrate a proof of concept for this approach by designing magnetoelastic machines whose motions are primarily guided by their magnetic energy landscapes and show that by operating near bifurcations we can achieve multiple transition pathways between states. This proof of concept demonstration illustrates the power of this approach, which could be especially useful for soft robotics and at the microscale where typical macroscale designs are difficult to implement.

bifurcation | design | meta-material | magnets

Significance

Systems composed of many interacting elements that collaboratively generate a function, such as meta-material robots, proteins, and neural networks are often not amenable to compartmentalized design: where individual modules each perform a distinct subfunction and are composed to create a complex function. Here, we pursue an alternative design paradigm where the function of machines arises from interactions of all the machine components, and the operation of the machine is organized by a bifurcation of multiple equilibria. These special points allow for robustly cycling between multiple distinct states by a small change of only a few control parameters. We illustrate this approach on a simple magnetoelastic machine and discuss its implications for the design of microscopic robots and protein-based machines.

Systems composed of a large number of interacting elements such as meta-materials, elastic membranes, and proteins can exhibit emergent behaviors that arise from the collaborative interaction of the system components. Designing functionality in such systems is a formidable task that requires searches in a high dimensional parameter space of the system components and their interactions. Developing organizing principles for effectively designing such systems remains an outstanding problem in the field (1–6). Here, we propose that designing multistate machines around bifurcations of multiple equilibria is a powerful paradigm that can be used to systematically organize such searches.

Cusp bifurcations where a single equilibrium splits into three equilibria as a function of a control parameter are a canonical dynamical systems structure (7) that has been used to explain various natural phenomena ranging from phase transitions (8) to the operation of simple machines. For example, it has been shown that Venus flytraps and hummingbird beaks open smoothly and then snap shut by operating about a cusp bifurcation (9, 10). Generalizations of cusp bifurcations have been proposed in René Thom's catastrophe theory to capture the essence of sharp state variations in multiple complex phenomena (11). The first of these "catastrophes" (saddle-node, cusp, swallowtail, and butterfly) are bifurcations of multiple equilibria where a single equilibrium splits into many equilibria due to a change in the system's parameters, as shown in Fig. 1*C* as well as in Salvador Dali's last painting depicting the swallowtail bifurcation of 4 equilibria (12).

Designing systems to operate near such bifurcations provides several advantages. Since the splitting of the equilibria has a power law dependence on the control parameters (13, 14), operating near bifurcations automatically provides a lever mechanism by which small variations in the control parameters lead to large changes in the system state (15, 16). In the case of the Venus fly trap, slight changes in hydrostatic pressure can drive large motions of the trap. Similarly in hummingbirds, slight twisting of the jaw bones enables rapid closing of a wide open beak. Further, as parameters are varied, the behavior in a neighborhood of a bifurcation of multiple equilibria unfolds into a geometrical arrangement of lower-order bifurcations, which are universally described by an analytic change of variables to a "normal form"(17–19). The robustness of systems operating through transitions between multiple states around a bifurcation of multiple equilibria is ensured by the topological structure of these unfolded lower-order bifurcation manifolds. As such, provided that the system trajectory encircles the cusp bifurcation where the saddle-node manifolds meet, the system is guaranteed to exhibit a smooth change in state followed by a snap. In the Venus fly trap and hummingbird examples, this topological protection guarantees that the opening and snapping of the trap or beak is

Author affiliations: [a]Laboratory of Atomic and Solid State Physics, Cornell University, Ithaca, NY 14853; and [b]Kavli Institute at Cornell for Nanoscale Science, Cornell University, Ithaca, NY 14853

Author contributions: P.L.M., J.P.S., I.C., and I.G. designed research; T.Y., D.H., Y.C., and I.G. performed research; T.Y., D.H., and I.G. analyzed data; and T.Y., D.H., P.L.M., J.P.S., I.C., and I.G. wrote the paper.

The authors declare no competing interest.

This article is a PNAS Direct Submission.

[1]T.Y. and D.H. contributed equally to this work.

[2]To whom correspondence may be addressed. Email: griniasty@cornell.edu.

This article contains supporting information online at https://www.pnas.org/lookup/suppl/doi:10.1073/pnas.2300081120/-/DCSupplemental.

Published August 14, 2023.

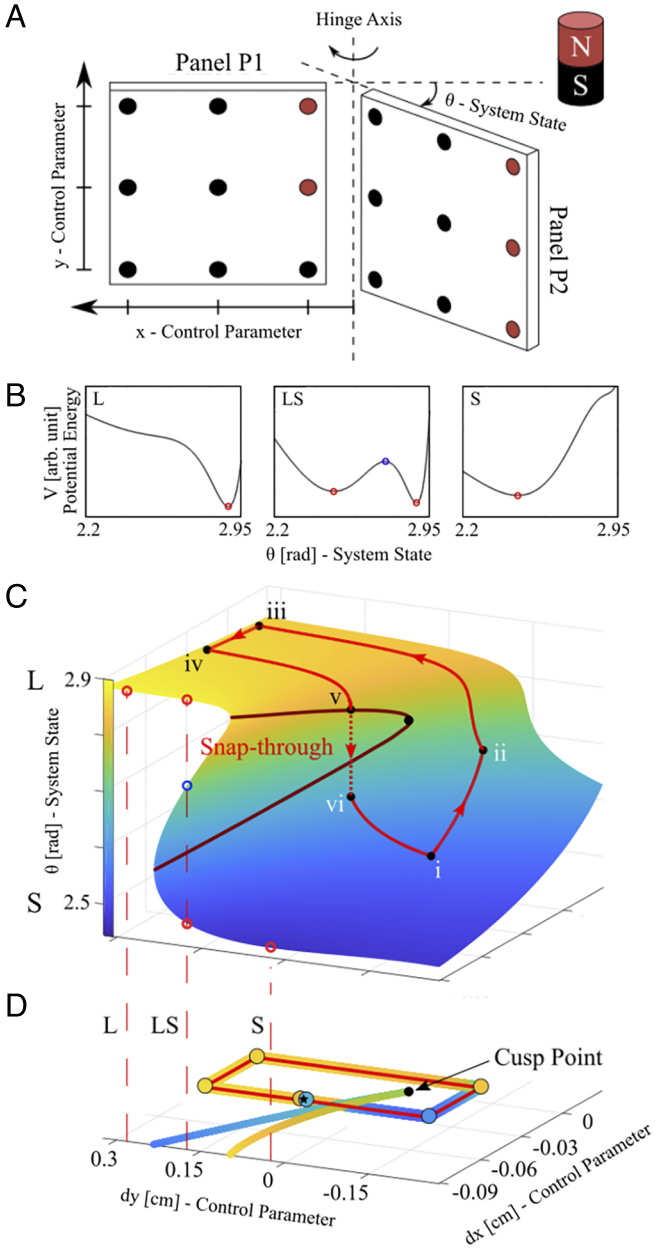

Fig. 1. Magnetoelastic machine capable of adopting multiple configurations due to operating near a cusp bifurcation. (*A*) *System*: Panels P1 and P2 are decorated with identical magnets with orientations denoted by their colors. Panel P1 is actuated externally to translate in the x and y directions, in response Panel P2 rotates about a hinge. The dynamics are overdamped. (*B*) *Magnetic potential energy landscapes*: We plot the potential for $dx = -0.09$ and $dy \in [0.28, 0.17, 0.02]$, where dx and dy are deviations from the cusp's position. Here, L and S denote two distinct states with relatively large and small θ magnitudes, respectively. Varying dy we cross two saddle-node bifurcations where the number of extrema of the magnetoelastic landscape changes. (*C*) *Equilibrium manifold*: The system's equilibria $\theta(dx, dy)$ are plotted as a function of the deviation of the parameters, with color signifying the value of θ. Brown curve marks saddle-node bifurcations where the number of equilibria change, and the light red curve denotes the experimental trajectory. (*D*) *Experimentally observed snap-through transition*: The system follows a parametric trajectory marked by a red curve and a tube whose color denotes the predicted state θ around a cusp bifurcation. The colored disks represent the experimental measurements. As expected, a single snap-through transition (denoted by $\star$) at a saddle-node bifurcation (curves colored according to the bifurcating state θ, which converges at the cusp) is observed.

robust against variations in the applied hydrostatic or muscle forces driving the transitions in the system state. Here, we propose that moving beyond cusp bifurcations to design systems that operate near bifurcations of arbitrarily many equilibria preserves the lever advantage and topological protection of cusp bifurcations. Such systems can be driven by only a few control parameters to undergo snapping transitions between multiple states, making the design of machines near such bifurcations a powerful paradigm for organizing complex functions. However, current software packages permit the design and analysis of systems operating near bifurcations of three or fewer equilibria (20–24). To develop and demonstrate this paradigm we introduce an algorithm that allows the efficient design of machines operating near bifurcations of multiple equilibria. We then experimentally investigate increasingly sophisticated magnetoelastic machines whose function is organized by such bifurcations.

We start by constructing a simple magnetoelastic machine consisting of a control panel that can be translated in the x–y plane and a second panel that is free to rotate about a hinge connecting the two panels (Fig. 1*A* and experimental apparatus

schematic *SI Appendix*, Fig. S1). The state of the system is given by the angle θ between the panels. By decorating the panels with magnets, we are able to design a magnetoelastic landscape with different numbers of minima as a function of the parameters x and y (Fig. 1*B*). Transitions between these minima correspond to changes in the state of the system. We denote the states L (large) and S (small) corresponding to the magnitude of the state variable. To understand the various pathways for making such transitions, we construct the manifold defined by the local equilibria as a function of the parameters x and y. For this particular arrangement of magnets, we calculate (*SI Appendix*) that the resulting manifold has a domain with multiple solutions delineated by saddle-node bifurcation curves (Fig. 1*C*, brown). These curves intersect and terminate at a cusp bifurcation beyond which there is only a single equilibrium state. By translating the control panel in the x–y plane, the system can undergo either smooth or abrupt changes in θ. For example, starting the system at point (i) and moving through points (ii–v), the hinge angle changes smoothly. A further slight decrease in the control parameter y, however, leads to an abrupt transition from a large to a small angle, corresponding to points (v) and (vi), respectively. These predictions are born out by the experiments (Fig. 1*D*), which also show a smooth change in θ for a pathway that encircles the cusp (i–v) and an abrupt transition in θ when crossing a saddle-node curve (v–vi). In this 2D representation the system makes a transition when the color of the path (yellow) matches the color denoting the state associated with the saddle-node curve (yellow). This magnetoelastic mechanism is reminiscent of the cocking and snapping of a Venus flytrap or a hummingbird's beak.

In addition to providing a mechanism for abrupt transitions, operating near a cusp bifurcation creates a lever mechanism where small variations in the control parameters lead to large variations in the system state. This mechanism resolves the generic problem that creating large variations in the system state often requires unfeasibly large variations in the control parameters. Lever mechanisms are generic near bifurcations of equilibria since the magnitude of the transition in the system state is typically proportional to the square root of the parameter distance from the bifurcation (*SI Appendix*).

To characterize this lever mechanism in our experiment, we map the snapping transition curves associated with the saddle-node bifurcations. Specifically, for a given value of y (or x), we toggle x (or y) so that the system snaps back and forth and records the values of the control parameters x and y, and system state θ immediately after each transition (Fig. 2*A*).

To test the scaling relations, we first define parameters dx, dy as displacements of x and y from the cusp. The normal form parameters a_1 and a_2 are then given by rescaled rotations of dx and dy (as shown in Fig. 2*A*). We then fit the predicted scaling form $\delta\theta \propto \sqrt{a_2}$ and $a_1 \propto a_2^{3/2}$ near a cusp to determine the cusp's position and the rotation of the normal form parameters (Fig. 2*B*). The fitted model then predicts that $\delta\theta \propto a_1^{1/3}$ (see *SI Appendix* and refs. 14 and 25 for derivations of these scaling laws). Because the scaling exponents for $\delta\theta$ are fractions of unity, small variations of the parameters along a_1 and a_2 lead to large variations of the system state. For example, in our experiments, the range of actuation for panel P1's position is approximately 1 cm and the range of angles accessible to panel P2 is 180° or π radians. Near the bifurcation, a translation along a_1 of 0.1% of its range (∼10 μm) leads to a snap that changes θ by ∼5% of its range (∼0.1 rad), providing a lever advantage of ∼50 (Fig. 2*B*).

The complexity of the actions achieved by such magnetoelastic mechanisms is dictated by the range and number of stable states that the system can access. This complexity can be achieved by designing the magnetoelastic potentials such that the system operates near bifurcations between multiple states. For example, working near a hypothetical symmetric butterfly bifurcation

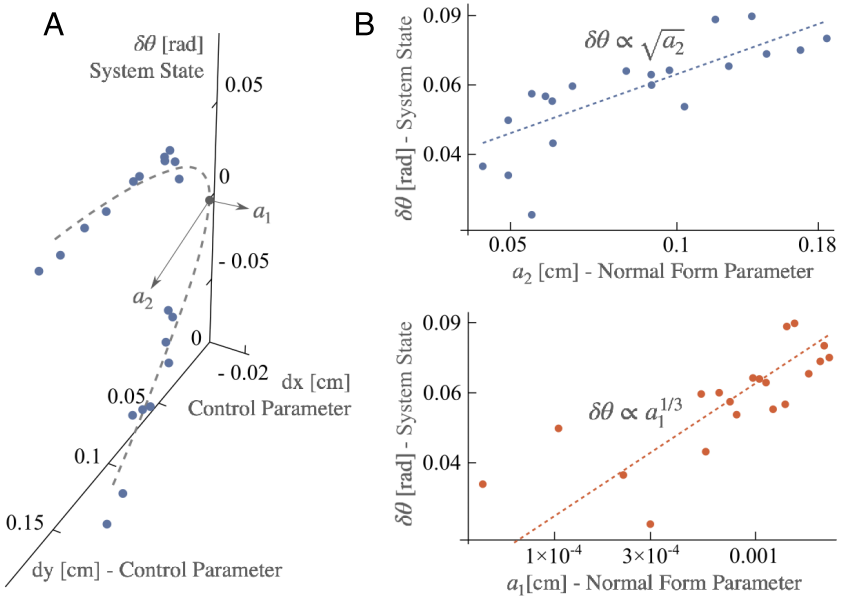

Fig. 2. Parametric levers. The change in the state of the system after a snap-through transition near a cusp bifurcation scales sublinearly with the normal form parameters. This sublinear scaling leads to large variation of the state in response to small variations of the system parameters. (*A*) *Measurements of snap-through transitions near a cusp:* The blue points mark the state of the magnetoelastic system of Fig. 1 after a snap-through transition. The dashed curve is a fit of snap-through transitions near a cusp bifurcation to the data, derived from the normal form potential $\tilde{V} = \delta\theta^4 + a_2\delta\theta^2 + a_1\delta\theta$. The normal form parameters a_1 and a_2 are locally given by re-scaled rotations of dx and dy, which are the deviations of the parameters away from the cusp. (*B*) *Scaling laws near a cusp:* The predicted scaling laws are demonstrated by projecting the measurements and fit onto log–log plots. Near the cusp the system response to a_1 acts as a giant lever, $\partial\delta\theta/\partial a_1 \sim 50$.

associated with the potential $V = \theta^6 + a_4\theta^4 + a_2\theta^2 + a_1\theta$ (with $a_3 = 0$) should enable smooth and abrupt transitions between three stable states in any order depending on the chosen trajectory for the control parameters. In Fig. 3*A*, we show a cut-through parameter space of the saddle-node surfaces near this butterfly bifurcation. If the system starts in the S (Small) state and moves along the depicted work cycle (black arrows), it would first snap to the M (Medium) state when the system crosses the purple saddle-node bifurcation and then the L (Large) state when it crosses the green curve. For the return path, however, the system would transition from the L minimum directly to the S minimum when it crosses the yellow saddle-node bifurcation curve. Moreover, by working near the bifurcation, the lever mechanism should allow for transitioning between these distinct states within an accessible range of experimental control parameters.

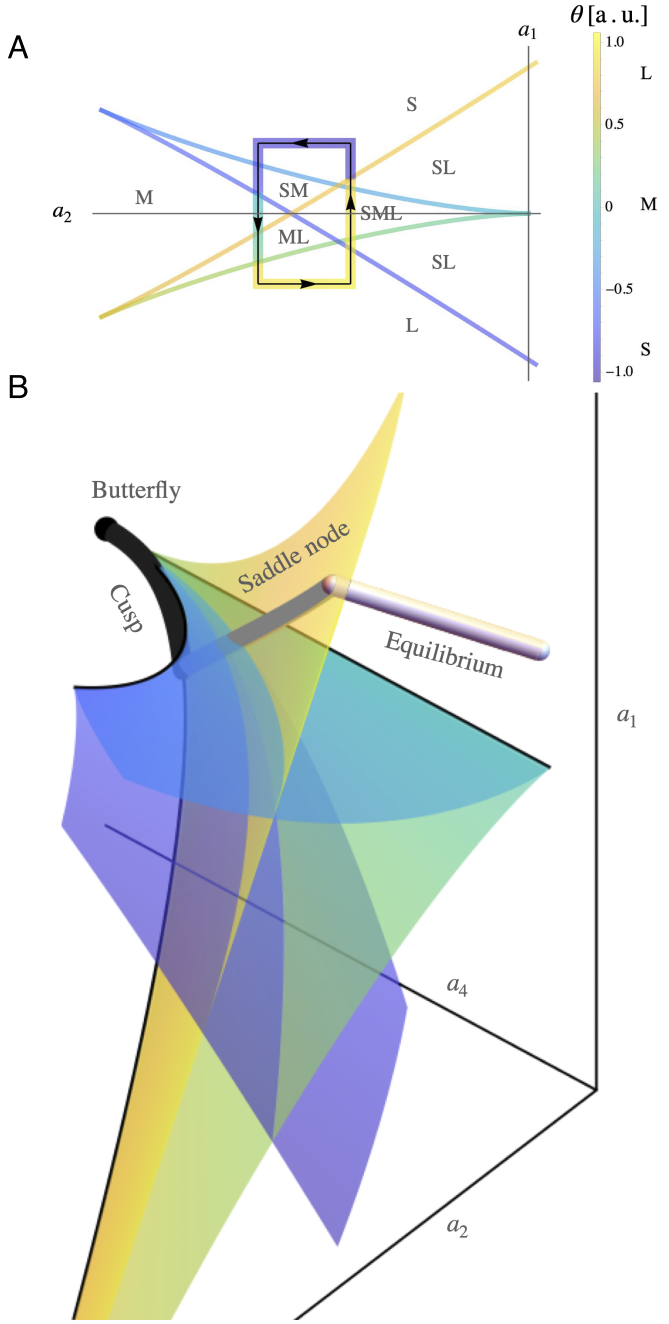

Fig. 3. Bifurcations of multiple equilibria. (*A*) *Work cycle near a butterfly*: A system operating near a hypothetical symmetrized butterfly bifurcation can cycle between three states. The bifurcation is associated with the potential $V = \theta^6 + a_4\theta^4 + a_2\theta^2 + a_1\theta$ and three accessible states denoted by large (L), medium (M) and small (S). As the system follows the trajectory denoted by black arrows, with colored background marking its state θ, it cycles between the three states snapping from S to M to L and back to S by changing a_2 and a_1 while $a_4 = 0.1$. The snaps occur at saddle-node bifurcations (colored curves) whose color signifies the state θ of the minima that is annihilated at each boundary. (*B*) *Gradient Continuation algorithm*: The search algorithm finds bifurcations of multiple equilibria by following a one-dimensional curve. Starting from a bifurcation of k equilibria, the algorithm searches for a bifurcation of $k+1$ equilibria by following a curve in the augmented parameter space, tangent to the gradient of $|V^{k+1}|$ in the k^{th} bifurcation manifold. We draw a search for a butterfly bifurcation in its symmetric normal form potential. The entire volume denotes the equilibrium manifold. Starting from a fixed point, the algorithm finds a saddle-node bifurcation (along the white curve). Parameters are then varied on the saddle-node surface (yellow), and cusp surface (thin black lines) to, respectively, find a cusp bifurcation (along the gray curve) and a swallowtail bifurcation (along the black curve) near a butterfly bifurcation (black point).

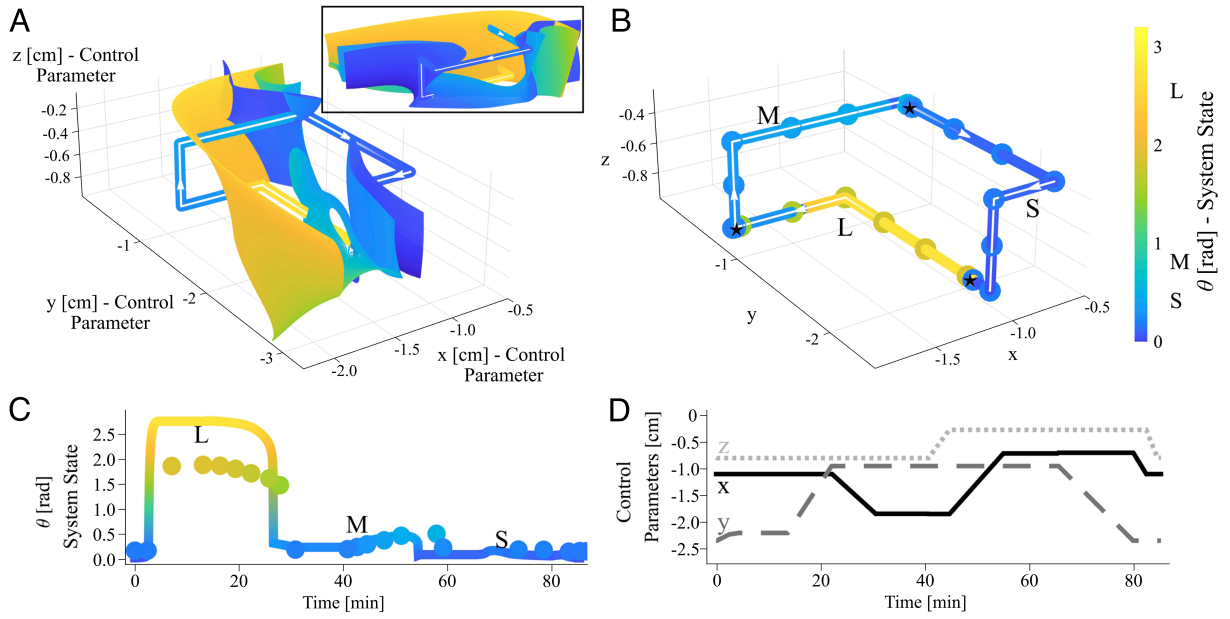

Fig. 4. 3-state cycle near butterfly bifurcation point. (*A*) *Theoretical design space*: The saddle-node surfaces of a magnetoelastic system with three active control parameters, *x*, *y*, and *z* are plotted, their color denotes the angle θ at which the snap occurs. The system's magnetic pattern is designed using the gradient continuation algorithm such that it operates near a butterfly bifurcation where multiple saddle-node surfaces coalesce, enabling multiple snap-through transitions at the surfaces. A trajectory (colored tube with white arrows) is chosen such that the system snaps in cycles between three states Large (L), Medium (M), and Small (S) angles. The system's predicted state is denoted by the tube's color. At intersections of the trajectory with a surface where their colors match the system is predicted to snap to a new state. The inset shows the same surface and trajectory from a different viewpoint (rotated by approximately 60°). (*B*) *Experimental control trajectory*: The colored disks mark the experimental measurements at various points along the designed trajectory. We observe three distinct transitions in the experiment (indicated by ⋆) as predicted. (*C*) *Experimental time series*: Dots mark the measured system state, and the line represents the theoretically predicted system state as a function of the control parameters, which change according to the experimental control sequence. (*D*) *Experimental control sequence*: Curves depict the variation of the control parameters, *x, y* and *z* as a function of time. *Remark*: Experiment and theory are also demonstrated in supplemental Movie S1. Traversing the same trajectory in the opposite direction leads to cyclic snaps between the Large and Small states as depicted in *SI Appendix*, Fig. S4 and Movie S2.

Search Algorithm for Bifurcations of Multiple Equilibria

To design parametric configurations corresponding to bifurcations of multiple equilibria, we develop a gradient continuation search algorithm that takes advantage of their nested structure. Bifurcations associated with *k* equilibria (minima plus maxima) are degenerate singularities where the first *k* derivatives of the potential vanish.* The first ones are the so-called saddle node, cusp, swallowtail, and butterfly bifurcations, which involve 2, 3, 4, and 5 equilibria, respectively. These bifurcations can be found iteratively by searching for singularities of the potential with increasing order, solving for one constraint at a time. We find that this method is especially efficient in finding experimentally realizable parametric configurations corresponding to bifurcations of multiple equilibria. Moreover, this method naturally extends to searching for bifurcations with desired properties by introducing further constraints, for example, optimizing the robustness of the bifurcation's associated states to external noise.

Minimizing the third derivative within the saddle-node manifold maintains the first two constraints and allows for finding a cusp bifurcation associated with two stable equilibria. Successive iterations allow for identifying bifurcations between an increasing number of equilibria and eventually the butterfly bifurcation. Our gradient continuation algorithm adapts standard algorithms from the dynamical systems literature (17, 19) and retools them to locally follow the gradient of the unsatisfied constraint (see *SI Appendix* for further details). This allows access to bifurcations of arbitrarily many equilibria through a simultaneous variation of an arbitrary number of parameters, while current continuation packages give access to bifurcations of two and three equilibria by varying a single parameter at a time (20–24). We depict the resulting search path in Fig. 3*B*, which highlights the fact that, independent of the number of parameters, the search algorithm follows a 1D trajectory, which is organized by the nested structure of the intermediate bifurcations. These properties enable the algorithm to find realizable bifurcations for systems with hundreds of parameters.

Three States and the Butterfly Bifurcation

As a proof of concept for our approach, we demonstrate the construction and operation of a magnetoelastic machine with 3 stable states operating near a bifurcation of multiple equilibria. The first bifurcation that organizes 3 stable states is a butterfly bifurcation of 5 equilibria (3 minima and 2 maxima). The first step in designing such a machine is to implement our gradient continuation algorithm to design a magnetoelastic potential with a butterfly bifurcation. To realize a system operating near such a bifurcation where only three control parameters (*x*, *y*, *z* positions of panel P1) are actively varied, we allowed the algorithm to also determine the *x*, *y* positions of two of the nine magnets on panel P1.† With these seven parameters and by sampling different patterns of dipole orientations, the algorithm was able to identify

*In multidimensional systems, the vanishing of the derivatives is replaced by an equivalent set of constraints, such as the vanishing of the gradient of the potential and an eigenvalue of the Hessian at a saddle-node bifurcation (17). These bifurcations correspond to special linear Lie algebras as shown in Arnold's ADE classification of bifurcations (13).

†Typically, a butterfly bifurcation requires four control parameters to navigate between all of the stable states. Here, we have identified a nonlinear mapping of the three active control parameters (*x*, *y*, *z*) onto the four-dimensional space, which enables transitions between arbitrary minima.

multiple butterfly bifurcations that satisfied these criteria (see *SI Appendix* for details).

Having found an appropriate butterfly bifurcation, we use standard dynamical systems continuation algorithms (7, 17) to compute and plot the saddle-node surfaces in the control parameter space (x, y, z) near the bifurcation (Fig. 4). We find multiple distinct surfaces where the color denotes the angle θ at which the saddle-node bifurcation occurs.[‡] Instructed by these surfaces, we design a cyclic path through the parameter space such that the system snaps between the large, medium, and small minima. The path color at each point denotes the system state, θ. As with the cusp and symmetrized butterfly bifurcations depictions in Figs. 1*D* and 3*A*, transitions occur at intersections of the path and saddle-node surfaces where their colors match. We note that for the generic butterfly bifurcation, the surface structure can be quite complicated as shown by the two projections in Fig. 4*A*. Indeed, even a system operating near the simple-looking symmetrized butterfly bifurcation generally requires four control parameters to move only along the a_1 direction. Here, we successfully use only three control parameters x, y, and z, to design a pathway that cycles between the three states.

Using the design parameters determined by our search algorithm, we built a magnetoelastic machine similar to that depicted in Fig. 1*A*, but with a different magnetic dipole pattern and with two of the magnets in panel P1 displaced in the panel plane (*SI Appendix*). By following the theoretically predicted path, we found three snap-through transitions from small to large, large to medium, and medium to small (Fig. 4 *B* and *C* and Movie S1). Two of the transitions occurred at the predicted locations, while the large to medium transition was displaced by 0.4 cm from its predicted location. In addition, we found excellent fidelity between the predicted and measured angles θ for the equilibrium states. We also demonstrated that by simply reversing the direction of cycling, the system transitions between two distinct states (see *SI Appendix*, Fig. S4 and Movie S2), which shows the possibility of designing two distinct work cycles with the same pathway thanks to the complex structure of the saddle-node surfaces near the bifurcation point. Finally, when the system was taken apart and reassembled (see *SI Appendix* for details), we were able to reliably reproduce the transitions associated with the designed trajectories.

Discussion

The experimental validation of this design paradigm with a butterfly bifurcation of 5 equilibria strongly supports the conjecture that this framework could be extended to design systems performing increasingly sophisticated functions by operating near bifurcations with a growing number of equilibria. For example, the control panel and snapping hinge near a cusp exhibit nonreciprocal motions that allow unidirectional swimming [i.e., a Purcell swimmer (26)]. The tristability near the butterfly bifurcation could enable both turning and swimming, with higher-order bifurcations giving access to multiple axes of rotation. Potential energies with these increasingly rare bifurcations can be found efficiently, because the gradient continuation algorithm follows a one-dimensional search path. Moreover, the associated lever mechanisms provide a design feature where the operation of the machine will likely be confined to a small parameter volume, enabling the execution of these actions by realizable machines.

Microscopic magnetoelastic machines could prove to be a useful instance of design instructed by bifurcations of multiple equilibria. An important emerging strategy for manufacturing microscopic and soft machines is fabricating them using two-dimensional lithographic and printing techniques (27–31). Such fabrication techniques, however, restrict the implementation of compound mechanisms composed of springs, cogs, screws, etc. that are used to achieve complex actions in traditional macroscale machines. These lever mechanisms could be replaced with magnetoelastic mechanisms with lever advantages induced by bifurcations. Magnetic interactions are especially well suited for this purpose since they are long-ranged and not easily screened. This long range allows for global changes to the conformation in response to local actuation of system components.

Importantly, since bifurcations of multiple equilibria are notoriously sensitive to variations of parameters, there is a concern that a machine operating near such bifurcations will be very sensitive to environmental noise, such as thermal vibrations, as well as to fabrication precision. Indeed, close to a bifurcation, the sensitivity of the system to variations of certain combinations of the system parameters grows exponentially as the number of associated equilibria increases. Mathematically, this is captured by mapping the potential to a canonical normal form via a change of coordinates (14, 25, Section 36.6) (see *SI Appendix* for derivation). Practically, however, this increased sensitivity is often blunted outside of the infinitesimal environment of the bifurcation. At a finite distance from the bifurcation, the mapping to the normal form or its linearization will often cease to be valid because of other singularities of the potential or the nonlinear fall-off in the potential. This nonlinearity is especially pronounced in keplerian potentials such as that of magnetic interactions. Critically, the saddle-node manifolds coalescing at the bifurcation are generically preserved outside this radius of convergence as they are topologically protected and can only annihilate at a cusp or a bifurcation of more equilibria. Thus, operating a machine near a bifurcation of multiple equilibria, but at a finite distance from it, allows the design of trajectories that take advantage of the multiple saddle-node transitions associated with it, and their lever advantages, while avoiding the local exponential sensitivity. For example, our experimental system explores almost all of its dynamical range, transitioning between states separated by ∼2 radians in response to variation of the control parameters smaller than the system's microscopic length scale, i.e., the separation between the magnets on each panel.

Similarly, the sensitivity of a system designed near a bifurcation of multiple equilibria to external noise grows exponentially with the number of associated states. This growth in sensitivity arises from the decrease in the potential barriers between adjacent states. For example, in a potential with k equilibria where all the potential barriers are of equal height, and the minima are equally deep (such a potential is proportional to a Chebyshev polynomial of the first kind of order $k+1$), the barrier heights decay as 2^{-k}. This sensitivity seems prohibitive as we imagine implementing this design principle to create systems cycling between multiple states. Despite this increased sensitivity, however, we estimate that the strength of magnetic interactions assures that magnetoelastic systems are robust to thermal noise at the microscale. Specifically, in magnetoelastic systems, the potential is proportional to the dipole–dipole interaction strength $\mu_0\mu^2L^6/R^3$ of two magnets with magnetic dipole densities μ

[‡]There is further local data in the potential at a saddle-node surface that can instruct the design of a trajectory. For example the sign of the third derivative of the potential signals whether the state's angle will increase or decrease as it bifurcates. Moreover, the merging of saddle-node surfaces can also be delineated by plotting the cusp bifurcations. Here, we do not include this additional information for ease of viewing.

panel size L and typical distance between dipoles R. Thermal noise is then comparable to the magnetoelastic potential barrier height when the number of equilibria $k \sim \log_2\left(\frac{\mu_0 \mu^2 L^3/(R/L)^3}{k_b T}\right)$. The magnetic dipole densities μ are of order $10^6 A/m$ at the microscale (32). The smallest two-state door (equivalent to the device in Fig. 1*A*) that is robust to thermal noise is then $\sim$ .1 μm in size, approaching the size limit of 30nm for fabricating stable magnetic domains (33). Conversely, a 100-μm machine will become sensitive to thermal noise near a bifurcation of $\sim$ 40 equilibria, that is 20 distinct states compressed in a span of 100 degrees.

As we traverse a path in the vicinity of the butterfly bifurcation, we store energy in the system via operating the control panel, which is then dissipated by the response of the rotating panel. The efficiency of this energy conversion depends on the details of the control mechanism, but we can estimate the output work done by the free panel. If the system is controlled adiabatically, so that it is approximately at an equilibrium point at all times, the force (perpendicular to the plane of the rotating panel) is always zero, $F_\theta(\theta^*) = 0$. This is true along the entire cycle except at the saddle-node bifurcations where the system jumps between states on the equilibrium manifold. Energy (injected by the control mechanism) is stored during the adiabatic tuning toward the saddle-node surfaces, then dissipated through the snap to the new target state. The partitioning of the energy dissipation between different snaps in tristable systems depends on the details of the potential and control path but obeys similar scaling laws to the equilibrium and saddle-node manifolds: $W \sim a_{k-1}^{(k+1)/2}$ for a bifurcation of k equilibira, where a_{k-1} is the leading normal form coefficient, measuring the distance from the bifurcation point (see *SI Appendix* for derivation). This law shows a trade-off between work and system state lever advantage: For a given small variation in control parameters, higher-order bifurcations allow amplified responses but do less work.

Finally, the designs that we have implemented in this paper assume operation in a low Reynolds number regime where inertia can be neglected. In the macroscale implementation, this was achieved by attaching a damping panel immersed in a solution of glycerol. We expect our designs to work even better as these machines are implemented at smaller scales since the importance of inertia drops quadratically with the system size. Operation of a 100-μm-scale machine in water, for example, would enable the system to be in the low Re regime while operating at rates that are 1,000-fold faster than those in the macroscale experiment.

Conclusions

We have shown that the operation of multiparameter machines near bifurcations of multiple equilibria allows them to efficiently and robustly cycle between multiple conformations. Moreover, we developed a generic step-by-step framework to design and implement systems that operate near such bifurcations. Specifically, we 1) created a search algorithm that optimizes over fabrication and other system parameters to enable operation near such bifurcations; 2) mapped the manifold of saddle-node bifurcations to determine a useful trajectory for the machine operation; and 3) demonstrated the robustness of this approach by constructing and operating a magnetoelastic machine that can cycle and robustly snap between multiple distinct configurations in response to small variations of a few control parameters.

Importantly, this design approach and step-by-step implementation are generic: Dynamical systems and bifurcation theory focus on general mathematical structures that appear across domains. The cusp and butterfly bifurcations we targeted for our designs are part of the broad family of cuspoidal bifurcations (11, 13, 14, 19, 25) that govern how all gradient systems transition between different equilibria. The design of systems near cuspoidal bifurcations can also organize the dynamics of multidimensional and nongradient systems (see *SI Appendix* for extension of our algorithm to such systems). Moreover, nongradient systems also exhibit bifurcations that give rise to sustained oscillations, quasiperiodicity, and chaos. It has been proposed that these dynamic bifurcations also provide useful targets for designing controllable complex behaviors (34–36), although these applications are less thoroughly studied. The generality of the dynamical systems framework allows the application of our design approach to a wide range of systems with multiple interacting components. Such systems range from artificial proteins (3) and multistate transistors (37), where the interactions are electrodynamic, to neural networks [both biological (38, 39) and synthetic (40)] where the interactions are governed by network topology. In principle, any system with dynamics governed by differential equations could be tuned to operate near a high-order bifurcation point, if we have access to the correct design and control parameters.

Cycling between transitions in mechanical implementations of such systems can generate work or locomotion. If the system is overdamped, as is often the case in microscopic systems operating in fluids, work and locomotion can be achieved by coupling the system to mechanisms that break time reversal symmetry. These mechanisms include ratchets or cilia-like flexible rods (41). In the case of the magnetoelastic hinge described here, time reversal symmetry is broken by combining the smooth translations of the control panel with abrupt transitions in the state of the dynamic panel. In systems where the control variable is not a mechanical parameter, time reversal symmetry can be broken by using the angle as an effective dynamical variable governing a system with multiple degrees of freedom such as is often used to parameterize robot locomotion.

More broadly, it is interesting to consider the extension of our work to systems with a larger number of dynamical variables $(\theta_1, \theta_2, \ldots)$. Here, we envision that by working near bifurcations of multiple variables (e.g., elliptic umbilic bifurcations) one could organize snaps between states separated along multiple variables. Such designs require extending our search algorithm to multiple variables while maintaining its low-dimensional search path. Alternatively, one could design mechanisms based on multiple local bifurcations that are weakly coupled across the machine. For example, one bifurcation of n states could be used to control θ_1 while a second bifurcation of m states organizes the dynamics of the variable θ_2. By weakly coupling the panels, and hence the variables θ_1 and θ_2, the machine can transform between $n \times m$ states in a coordinated fashion. Indeed this approach is already being implemented for bifurcations with two states, where the multiple states are also used for computation and memory formation (42–44). Increasing the number of states associated with each variable would enable a similarly rich landscape for machine design with far fewer mechanical elements or panels.

Finally, it is interesting to consider whether this design paradigm can be used to understand natural systems beyond the Venus fly trap and hummingbird beak. For example, molecular machines such as proteins often transition between different configurations. It is interesting to consider whether such transitions can be thought of as snaps organized by bifurcations of many states (3, 6). As another example, bifurcation theory has been implemented to identify and explain epigenetic dynamics

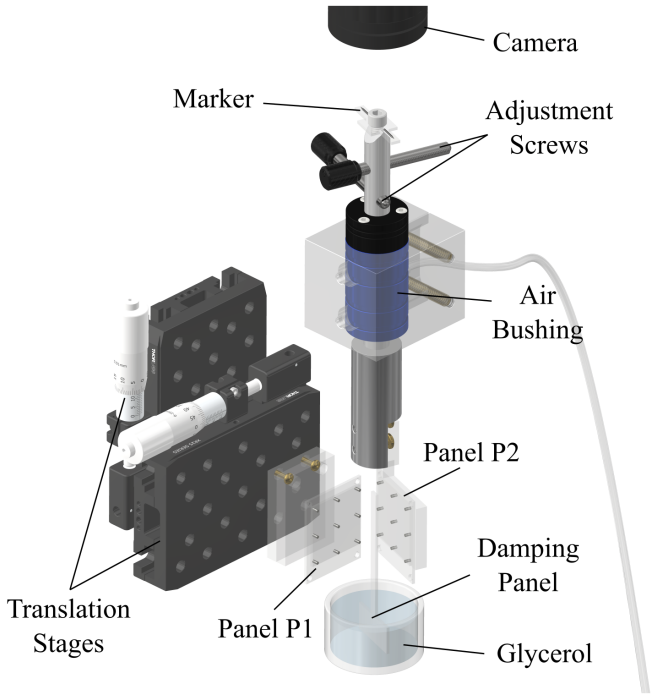

Fig. 5. Experimental setup. Sketch of the experimental system used for the demonstration of cycles and angle measurements. Panel P1 is attached to a set of translation stages which allows us to implement the spatial control parameters in all experiments. Panel P2 is attached to an air bushing that is fixed in space. An attachment submerged in glycerol is added to the base of Panel P2 to introduce damping to the system.

of cell differentiation (45–47). These approaches often focus on consecutive 2-state bifurcations. The results presented here, however, suggest that a comparably simple evolutionary pathway could entail development of multistate bifurcations. Such a structure could allow the addition of new states while maintaining the existing configuration through an evolutionary process, similar to the path taken by the gradient continuation algorithm.

Materials and Methods

Construction of Experimental Hinge System. Panel P1 is constrained to a set of linear translation stages that allow its position to be adjusted manually to any x or y coordinates near the cusp. For experiments near the butterfly bifurcation point, an extra translation stage is attached to Panel P1 to allow adjustment of its z coordinate. Panel P2 is attached to an OAV frictionless thrust air bushing with a 13-mm shaft. The air bushing is attached to a fixed metal housing to limit Panel P2 to its rotational degree of freedom. A T-shaped paddle is attached to the bottom of the shaft and immersed in glycerol to introduce damping to the system. Additionally, we position a Basler Ace aca3088-57um area scan camera above the center of the air bushing to take top-view images of the air bushing which are then used to calculate the angle response of Panel P2 to high precision. Full experimental schematic shown in Fig. 5.

Panels for Experiments near Cusp Point. Each magnetic panel is constructed using two 1/16 in thick laser-cut acrylic pieces and nine grade N48 neodymium magnets of diameter 1/16 in and height 1/8 in. Magnets are arranged in a 3-by-3 square lattice with a lattice constant of 1.5 cm.

Panels for Experiments near Butterfly Point. Each magnetic panel is constructed using two 1/16 in thick laser-cut acrylic pieces and nine grade N48 neodymium magnets of diameter 1/8 in and height 1/8 in. Magnets are arranged in a 3-by-3 square lattice with lattice constant of 2.5 cm. In panel P1, the x, y position of two of the magnets is displaced according to the design determined by the search algorithm. The two magnets whose position is offset are the magnet in the bottom row on the right column, whose offsets are $dx1 = 1.418$ cm, $dy1 = -0.273$ cm, and the magnet in the middle row on the left column, with offsets $dx2 = -0.826$ cm, $dy2 = -0.986$ cm. A technical drawing illustrating the panels used for the butterfly experiment is included in *SI Appendix*.

Angle Measurements. A marker is attached to the top of the air bushing, and a camera records the location of the marker during the experiment. At each given time, the measured angle is the determined by three points: current marker location, location of the center of rotation, and marker location at $\theta = 0$. We calibrate the system by recording the location of the pixel at $\theta = 0$ and several other distinct angles. The pixel location corresponding to the center of rotation is obtained using a fitted circle through the calibration data points. The resulting angle is then deduced from the three measured points. This data collection process is conducted in MATLAB.

Data, Materials, and Software Availability. All study data are included in the article and/or supporting information.

ACKNOWLEDGMENTS. We thank Michael Brenner, Chrisy Xiyu Du, Yan Yang, Robert Distasio, and John Guckenheimer for inspiring discussions. This work was financially supported primarily by NSF Grant DMREF-89228, NSF Grant EFRI-1935252, NSF Grant CBET-2010118, Cornell Center for Materials Research DMR-1719875, and by Air Force Office of Scientific Research Grant MURI: FA9550-16-1-0031. I.G. was also supported by the Cornell Laboratory of Atomic and Solid State Physics and Eric and Wendy Schmidt AI in Science Postdoctoral Fellowship. D.H. was supported by an NSF Graduate Research Fellowship Grant No. DGE-2139899.

1. O. Sigmund, K. Maute, Topology optimization approaches. *Struct. Multidiscip. Opt.* **48**, 1031–1055 (2013).
2. C. P. Goodrich, A. J. Liu, S. R. Nagel, The principle of independent bond-level response: Tuning by pruning to exploit disorder for global behavior. *Phys. Rev. Lett.* **114**, 225501 (2015).
3. P. S. Huang, S. E. Boyken, D. Baker, The coming of age of de novo protein design. *Nature* **537**, 320–327 (2016).
4. J. W. Rocks *et al.*, Designing allostery-inspired response in mechanical networks. *Proc. Natl. Acad. Sci. U.S.A.* **114**, 2520–2525 (2017).
5. V. F. Hagh, S. R. Nagel, A. J. Liu, M. L. Manning, E. I. Corwin, Transient learning degrees of freedom for introducing function in materials. *Proc. Natl. Acad. Sci. U.S.A.* **119**, e2117622119 (2022).
6. J. P. Eckmann, J. Rougemont, T. Tlusty, Colloquium: Proteins: The physics of amorphous evolving matter. *Rev. Mod. Phys.* **91**, 031001 (2019).
7. J. Guckenheimer, Y. A. Kuznetsov, Cusp bifurcation. *Scholarpedia* **2**, 1852 (2007).
8. R. K. Pathria, *Statistical Mechanics* (Elsevier, 2016).
9. Y. Forterre, J. M. Skotheim, J. Dumais, L. Mahadevan, How the Venus flytrap snaps. *Nature* **433**, 421–425 (2005).
10. M. Smith, G. Yanega, A. Ruina, Elastic instability model of rapid beak closure in hummingbirds. *J. Theor. Biol.* **282**, 41–51 (2011).
11. R. Thom, *Structural Stability and Morphogenesis* (CRC Press, 1989).
12. S. Dali, The Swallow's Tail–Series of Catastrophes (1983). https://www.salvador-dali.org/en/artwork/catalogue-raisonne-paintings/obra/1013/untitled-swallow-s-tail-and-cellos-the-catastrophes-series (Accessed 1 April 2023).
13. V. I. Arnol'd, Ed., *Bifurcations of Equilibria* (Springer, Berlin/Heidelberg, Germany, 1994), pp. 10–38.
14. M. V. Berry, Focusing and twinkling: Critical exponents from catastrophes in non-Gaussian random short waves. *J. Phys. A: Math. General* **10**, 2061–2081 (1977).
15. J. T. Overvelde, T. Kloek, J.J. D'haen, K. Bertoldi, Amplifying the response of soft actuators by harnessing snap-through instabilities. *Proc. Natl. Acad. Sci. U.S.A.* **112**, 10863–10868 (2015).
16. Y. Chi, Y. Hong, Y. Zhao, Y. Li, J. Yin, Snapping for high-speed and high-efficient butterfly stroke–like soft swimmer. *Sci. Adv.* **8**, eadd3788 (2022).
17. Y. A. Kuznetsov, *Topological Equivalence, Bifurcations, and Structural Stability of Dynamical Systems* (Springer, New York, NY, 2004).
18. J. W. Bruce, P. J. Giblin, *Curves and Singularities: A Geometrical Introduction to Singularity Theory* (Cambridge University Press, ed. 2, 1992).
19. J. Guckenheimer, P. Holmes, *Nonlinear Oscillations, Dynamical Systems, and Bifurcations of Vector Fields* (Springer, New York, NY, 1983).

20. R. H. Clewley, W.E. Sherwood, M.D. LaMar, *Pydstool, A Software Environment for Dynamical Systems Modeling* (JM Guckenheimer, 2007).
21. W. Govaerts, Y. A. Kuznetsov, B. Sijnave, "Continuation of codimension-2 equilibrium bifurcations" in *Content in Numerical Methods for Bifurcation Problems and Large-scale Dynamical Systems* (Springer, 2000), pp. 163–184.
22. A. Dhooge, W. Govaerts, Y. A. Kuznetsov, MATCONT: A MATLAB package for numerical bifurcation analysis of odes. *ACM Trans. Math. Software (TOMS)* **29**, 141–164 (2003).
23. E. J. Doedel *et al*., AUTO-07p: Continuation and Bifurcation Software for Ordinary Differential Equations (2007). http://cmvl.cs.concordia.ca/auto/#documentation (Accessed 1 January 2023).
24. B. Ermentrout. "XPPAUT" in *Computational Systems Neurobiology*, N. Le Novére, Eds. (Springer, Dordrecht, 2012), pp. 519–531.
25. DLMF, NIST Digital Library of Mathematical Functions, Version 1.1.10. http://dlmf.nist.gov/36.6. Accessed 1 January 2023.
26. E. M. Purcell, Life at low Reynolds number. *Am. J. Phys.* **45**, 3–11 (1977).
27. J. Kim, J. A. Hanna, M. Byun, C. D. Santangelo, R. C. Hayward, Designing responsive buckled surfaces by halftone gel lithography. *Science* **335**, 1201–1205 (2012).
28. T. H. Ware, M. E. McConney, J. J. Wie, V. P. Tondiglia, T. J. White, Voxelated liquid crystal elastomers. *Science* **347**, 982–984 (2015).
29. J. H. Na *et al*., Programming reversibly self-folding origami with micropatterned photo-crosslinkable polymer trilayers. *Adv. Mater.* **27**, 79–85 (2015).
30. A. Sydney Gladman, E. A. Matsumoto, R. G. Nuzzo, L. Mahadevan, J. A. Lewis, Biomimetic 4D printing. *Nat. Mater.* **15**, 413 EP (2016).
31. M. Z. Miskin *et al*., Electronically integrated, mass-manufactured, microscopic robots. *Nature* **584**, 557–561 (2020).
32. J. Cui *et al*., Nanomagnetic encoding of shape-morphing micromachines. *Nature* **575**, 164–168 (2019).
33. R. Niu *et al*., Magnetic handshake materials as a scale-invariant platform for programmed self-assembly. *Proc. Natl. Acad. Sci. U.S.A.* **116**, 24402–24407 (2019).
34. C. Scheibner, M. Fruchart, V. Vitelli, Soft metamaterials: Adaptation and intelligence. arXiv [Preprint] (2022). http://arxiv.org/abs/2205.01867 (Accessed 1 January 2023).
35. M. Brandenbourger, C. Scheibner, J. Veenstra, V. Vitelli, C. Coulais, Limit cycles turn active matter into robots. arXiv [Preprint] (2021). http://arxiv.org/abs/2108.08837 (Accessed 1 January 2023).
36. C. Weis *et al*., Coalescence of attractors: Exceptional points in non-linear dynamical systems. arXiv [Preprint] (2022). http://arxiv.org/abs/2207.11667 (Accessed 1 January 2023).
37. D. U. Lim, S. B. Jo, J. Kang, J. H. Cho, Multi-state heterojunction transistors based on field-effect tunneling-transport transitions. *Adv. Mater.* **33**, 2101243 (2021).
38. P. Érdi, T. Gröbler, K. Kaski, "Dynamic phenomena in the olfactory bulb: I. Bifurcation sequences, coexistence of periodicity and chaos, synaptic modification induced transitions" in *Artificial Neural Networks* (Elsevier, 1992), pp. 873–876.
39. P. Érdi, T. Grőbler, G. Barna, K. Kaski, Dynamics of the olfactory bulb: Bifurcations, learning, and memory. *Biol. Cybern.* **69**, 57–66 (1993).
40. L. Medsker, L. C. Jain, *Recurrent Neural Networks: Design and Applications* (CRC Press, 1999).
41. E. Lauga, Life around the scallop theorem. *Soft Matter* **7**, 3060–3065 (2011).
42. C. Coulais, A. Sabbadini, F. Vink, M. van Hecke, Multi-step self-guided pathways for shape-changing metamaterials. *Nature* **561**, 512–515 (2018).
43. H. Bense, M. van Hecke, Complex pathways and memory in compressed corrugated sheets. *Proc. Natl. Acad. Sci. U.S.A.* **118**, e2111436118 (2021).
44. D. Shohat, D. Hexner, Y. Lahini, Memory from coupled instabilities in unfolded crumpled sheets. *Proc. Natl. Acad. Sci. U.S.A.* **119**, e2200028119 (2022).
45. D. A. Rand, A. Raju, M. Sáez, F. Corson, E. D. Siggia, Geometry of gene regulatory dynamics. *Proc. Natl. Acad. Sci. U.S.A.* **118**, e2109729118 (2021).
46. E. Marco *et al*., Bifurcation analysis of single-cell gene expression data reveals epigenetic landscape. *Proc. Natl. Acad. Sci. U.S.A.* **111**, E5643–E5650 (2014).
47. M. Setty *et al*., Wishbone identifies bifurcating developmental trajectories from single-cell data. *Nat. Biotechnol.* **34**, 637–645 (2016).